Contribution of the receptor guanylyl cyclase GC-D to chemosensory function in the olfactory epithelium

Trese Leinders-Zufall*, Renee E. Cockerham†, Stylianos Michalakis‡, Martin Biel‡, David L. Garbers§, Randall R. Reed¶, Frank Zufall*‖, and Steven D. Munger†**

*Department of Physiology, University of Saarland School of Medicine, 66421 Homburg/Saar, Germany; †Department of Anatomy and Neurobiology and Program in Neuroscience, University of Maryland School of Medicine, Baltimore, MD 21201; ‡Munich Center for Integrated Protein Science and Department of Pharmacy, Center for Drug Research, Ludwig-Maximilians-Universität München, 81377 Munich, Germany; §Department of Pharmacology and the Cecil H. and Ida Green Center for Reproductive Biology Sciences, University of Texas Southwestern Medical Center, Dallas, TX 75390; and ¶Department of Molecular Biology and Genetics and Center for Sensory Biology, Johns Hopkins School of Medicine, Baltimore, MD 21205

Edited by Linda B. Buck, Fred Hutchinson Cancer Research Center, Seattle, WA, and approved July 26, 2007 (received for review May 25, 2007)

The mammalian main olfactory epithelium (MOE) recognizes and transduces olfactory cues through a G protein-coupled, cAMP-dependent signaling cascade. Additional chemosensory transduction mechanisms have been suggested but remain controversial. We show that a subset of MOE neurons expressing the orphan receptor guanylyl cyclase GC-D and the cyclic nucleotide-gated channel subunit CNGA3 employ an excitatory cGMP-dependent transduction mechanism for chemodetection. By combining gene targeting of *Gucy2d*, which encodes GC-D, with patch clamp recording and confocal Ca^{2+} imaging from single dendritic knobs *in situ*, we find that GC-D cells recognize the peptide hormones uroguanylin and guanylin as well as natural urine stimuli. These molecules stimulate an excitatory, cGMP-dependent signaling cascade that increases intracellular Ca^{2+} and action potential firing. Responses are eliminated in both *Gucy2d*- and *Cnga3*-null mice, demonstrating the essential role of GC-D and CNGA3 in the transduction of these molecules. The sensitive and selective detection of two important natriuretic peptides by the GC-D neurons suggests the possibility that these cells contribute to the maintenance of salt and water homeostasis or the detection of cues related to hunger, satiety, or thirst.

cGMP | natriuretic peptide | transduction | *Gucy2d* | CNGA3

Odor recognition by canonical olfactory sensory neurons (OSNs) of the main olfactory epithelium (MOE) begins when odor molecules bind to any one of many hundred G protein-coupled odorant receptors (1–4). Upon ligand binding, odorant receptors activate the G protein $G\alpha_{olf}$, which stimulates type III adenylyl cyclase to increase intracellular levels of cAMP (4–9). This second messenger then directly opens cAMP-sensitive, cyclic nucleotide-gated (CNG) channels in the plasma membrane, resulting in the initial depolarization of the cell (3, 4). OSNs that use this cAMP-mediated transduction cascade respond to a wide variety of odors, including food odors, volatile pheromones, and peptides that bind major histocompatibility complex proteins (4, 10–12). A recently discovered second family of G protein-coupled receptors expressed in the MOE, the trace amine-associated receptors, may also function in the recognition of some odors or pheromones by coupling to the canonical cAMP pathway (13). However, there has been intense debate as to whether the cAMP cascade is the only excitatory sensory transduction mechanism in the MOE (11, 14, 15).

A subpopulation of ciliated MOE neurons that express the orphan receptor guanylyl cyclase GC-D (16) are prime candidates to mediate cAMP-independent odor recognition. GC-D cells lack key components of the canonical OSN odor transduction cascade, including $G\alpha_{olf}$, type III adenylyl cyclase, the Ca^{2+}/calmodulin-dependent phosphodiesterase PDE1C2, the cAMP-specific phosphodiesterase PDE4A, and the cAMP-sensitive CNG channel subunits CNGA2 and CNGB1b (17, 18). Instead, these neurons express a cGMP-specific CNG channel subunit, CNGA3, and a cGMP-stimulated phosphodiesterase, PDE2 (17, 18). Although these cells were identified more than a decade ago (16), there is no functional evidence that they play a role in odor recognition. On the basis of their distinct molecular profiles and axonal targets in the olfactory bulb (OB) (16–18), GC-D cells have been suggested to respond to hormones or pheromones (18). However, it has not been possible to obtain physiological recordings from identified GC-D neurons. Consequently, no sensory stimuli detected by these cells are known, and the proposed chemosensory function of GC-D and the cells that express it remains elusive.

Results

Targeting of GC-D Neurons and the Necklace Glomeruli in Mice. To determine whether GC-D and the neurons that express it have a chemosensory role, we used gene targeting in embryonic stem cells to generate mice that lack this protein. Parts of exons 2 and 3 of the *Gucy2d* gene (19), encoding the bulk of the extracellular receptor domain of GC-D, were deleted and replaced by an IRES-*Mapt-lacZ* reporter cassette and *neo* selection cassette [supporting information (SI) Fig. 6 *A* and *B*]. Chimeric mice were generated, a breeding colony was established, and the selection cassette was excised by cre-mediated recombination. *Gucy2d* +/− and −/− mice displayed no obvious physical or behavioral abnormalities and were able to mate and suckle effectively (SI Fig. 7).

GC-D expression is specifically abolished in *Gucy2d* −/− mice. The GC-D message was amplified by RT-PCR from MOE cDNA of *Gucy2d* +/− but not −/− mice (SI Fig. 6*C*). The expression of two other markers of GC-D neurons, PDE2 (18) and CNGA3 (17), was unaffected. Only a small subset of MOE neurons in *Gucy2d* +/− and −/− mice express the β-galactosidase (β-gal) reporter (SI Fig. 6*D*), consistent with the small number of GC-D neurons reported previously (16). The axons of GC-D neurons innervate a small number of glomeruli in the caudal main OB, the necklace glomeruli (18), although the projection path of GC-D neuron axons

Author contributions: T.L.-Z., D.L.G., R.R.R., F.Z., and S.D.M. designed research; T.L.-Z., R.E.C., and S.D.M. performed research; T.L.-Z., R.E.C., F.Z., and S.D.M. analyzed data; T.L-Z., S.M., M.B., D.L.G., R.R.R., and S.D.M. contributed new reagents/analytic tools; and F.Z. and S.D.M. wrote the paper.

The authors declare no conflict of interest.

This article is a PNAS Direct Submission.

Abbreviations: CNG, cyclic nucleotide-gated; EHNA, erythro-9-[2-hydroxy-3-nonyl]-adenine; EOG, electroolfactogram; G, guanylin; IBMX, 3-isobutyl-1-methylxanthine; IHC, immunohistochemistry; MOE, main olfactory epithelium; OB, olfactory bulb; OSN, olfactory sensory neuron; PDE, phosphodiesterase; TH, tyrosine hydroxylase; UG, uroguanylin.

‖To whom correspondence may be addressed. E-mail: frank.zufall@uks.eu.

**To whom correspondence may be addressed at: Department of Anatomy and Neurobiology, University of Maryland School of Medicine, 20 Penn Street, S251, Baltimore, MD 21201. E-mail: smung001@umaryland.edu.

This article contains supporting information online at www.pnas.org/cgi/content/full/0704965104/DC1.

© 2007 by The National Academy of Sciences of the USA

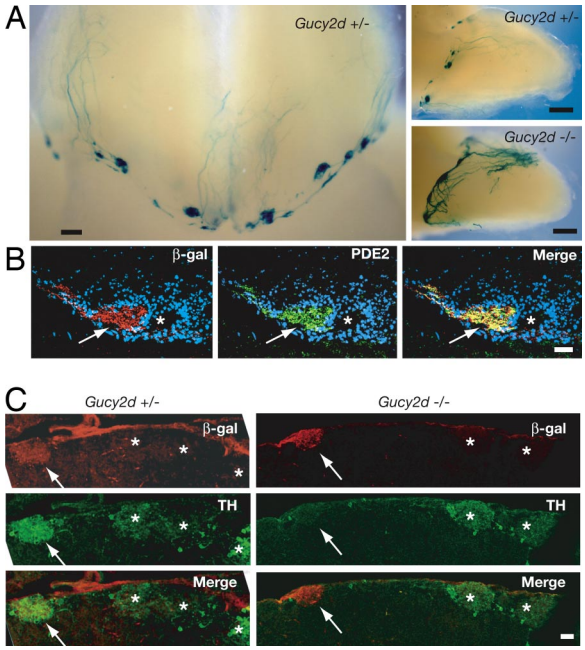

Fig. 1. Visualization of GC-D neurons and the necklace glomeruli. (*A*) Whole-mount X-Gal histochemistry of paired or right OBs from *Gucy2d* +/− (*Left* and *Upper Right*) and −/− (*Lower Right*) mice (all ventral views). (*Upper Right*) OB is the same as in the *Left*, although separated from the left OB. [Scale bars: 200 μm (*Left*), 500 μm (*Right*).] (*B*) β-Gal (red) and PDE2 (green) IHC in an OB from a *Gucy2d* −/− mouse; DAPI (blue) labels cell nuclei. Arrow, necklace glomerulus; asterisk, β-gal-negative glomerulus. (Scale bar: 100 μm.) (*C*) β-Gal (red) and TH (green) IHC in OBs of *Gucy2d* +/− (*Left*) and −/− (*Right*) mice. Arrows, necklace glomerulus; asterisks, β-gal-negative glomeruli. (Scale bar: 100 μm.)

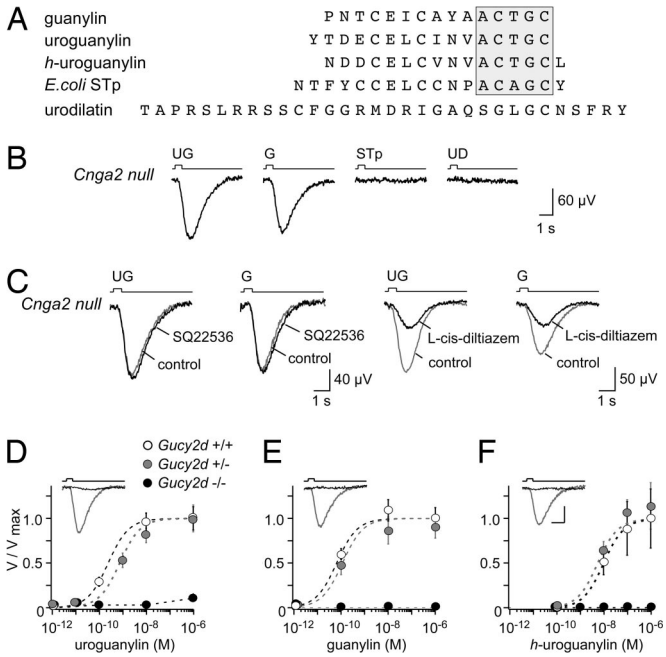

Fig. 2. Essential role of GC-D in olfactory recognition of guanylin family peptides. (*A*) Primary structure of peptide ligands used (single-letter amino acid codes). Guanylin (G), uroguanylin (UG), and urodilatin (UD) are mouse/rat isoforms; *h*-uroguanylin is the human isoform. The gray box indicates a peptide motif in common (27). G, UG, and STp are known ligands for the receptor guanylyl cyclase GC-C; urodilatin is a ligand for the related receptor GC-A. (*B*) Examples of local field potentials generated in the MOE of *Cnga2*-null mice, with 500-ms pulses of 1 μM UG or G. Stimulation with 1 μM STp or urodilatin failed to elicit a response. Results are representative of a total of six recordings in six *Cnga2*-null mice. Recordings in *Gucy2d* +/− mice gave the same results ($n = 9$). (*C*) UG- or G-evoked potentials are unaffected by treatment with the adenylyl cyclase inhibitor SQ22536 (300 μM, $n = 8$) but are suppressed reversibly by the CNG channel blocker L-*cis*-diltiazem (100 μM, $n = 6$). (*D–F*) Dose dependence of peak responses to UG (*D*), G (*E*), or *h*-UG (*F*) obtained from *Gucy2d* +/+, +/−, or −/− mice. Data points are normalized to the mean response of a given stimulus at 1 μM in *Gucy2d* +/+ mice (UG: 192.1 ± 24.8 μV, $n = 6$; G: 95.9 ± 11.2 μV, $n = 7$; *h*-UG: 105.9 ± 34.6 μV, $n = 7$); none was statistically significant in *Gucy2d* −/− mice. At least six independent measurements were obtained from three or four *Gucy2d* +/+ and +/− mice, respectively. Data from *Gucy2d* −/− mice are based on recordings from 11–23 MOE locations. Curves were fit by using the Hill equation [$K_{1/2}$ values: UG, 247 ± 11 pM (+/+), 769 ± 256 pM (+/−); G, 66.1 ± 15.5 pM (+/+), 116.2 ± 55.3 pM (+/−); *h*-UG, 9.86 ± 0.55 nM (+/+), 5.48 ± 1.48 nM (+/−)]. (*Insets*) Examples of the time course of peptide-induced responses in *Gucy2d* +/− or −/− mice (ligands 1 μM each). (Scale bars: 40 μV, 1 s.)

to the necklace glomeruli was unknown. Whole-mount X-Gal histochemistry of OBs from *Gucy2d* +/− and −/− mice revealed a diffuse group of β-gal-positive axons that project caudally from the MOE and along the ventrolateral aspects of the OB (Fig. 1*A* and SI Fig. 8). Upon reaching the caudal OB, these axons course dorsally on the medial and lateral surfaces to terminate in 9–11 superficial glomeruli that are consistent in number and position with the necklace glomeruli (20, 21). These β-gal-positive glomeruli exhibit a rough symmetry across the two OBs within animals (Fig. 1*A Left*). The level of β-gal expression is greater in *Gucy2d* −/− mice than in +/− mice (Fig. 1*A Right*), as would be expected by the presence of a second *lacZ* allele. However, the number and positions of β-gal-positive glomeruli in *Gucy2d* +/− and −/− mice are nearly identical (Fig. 1*A Right*), indicating that functional GC-D is not required for normal axonal targeting.

We next asked whether β-gal-positive neurons express a key molecular marker of GC-D neurons, PDE2. This phosphodiesterase, present in the somata, cilia, dendrites, and axons of GC-D neurons, is a specific marker of both GC-D neurons and the necklace glomeruli (18). We performed double-label immunohistochemistry (IHC) for β-gal and PDE2 in OBs of *Gucy2d* +/− and −/− mice. All glomeruli that were immunopositive for β-gal were also PDE2-positive (and vice versa) in both *Gucy2d* +/− and −/− mice (Fig. 1*B* and data not shown). Thus, expression of the β-gal reporter is restricted to GC-D neurons and the necklace glomeruli and serves as a specific marker for GC-D neurons in these gene-targeted mice.

The presence of normal afferent activity from the MOE to most OB glomeruli, although not the necklace glomeruli, depends on an intact cAMP signaling cascade (22). To provide an initial assessment of the necessity of GC-D expression for the maintenance of afferent activity in the necklace glomeruli, we took advantage of the observation that tyrosine hydroxylase (TH) expression in OB periglomerular cells is a correlate of afferent activity (22, 23). In *Gucy2d* +/− mice, both β-gal-positive and β-gal-negative glomeruli express TH (Fig. 1*C Left*). However, TH immunoreactivity is nearly absent in β-gal-positive glomeruli of *Gucy2d* −/− mice (Fig. 1*C Right*), suggesting that GC-D neurons provide functional innervation to the necklace glomeruli and that GC-D itself is necessary for normal afferent activity to these glomeruli.

MOE Responses to Uroguanylin Family Peptides Require GC-D. We next sought to determine whether GC-D neurons recognize distinct chemosensory cues. We focused on peptides found in urine (Fig. 2*A*) because other receptor guanylyl cyclases function as peptide receptors (24) and nonvolatile peptide stimuli have been shown to reach and activate the MOE after direct contact with a stimulus (10, 12). Because GC-D neurons lack components of the canonical olfactory cAMP signaling cascade, we

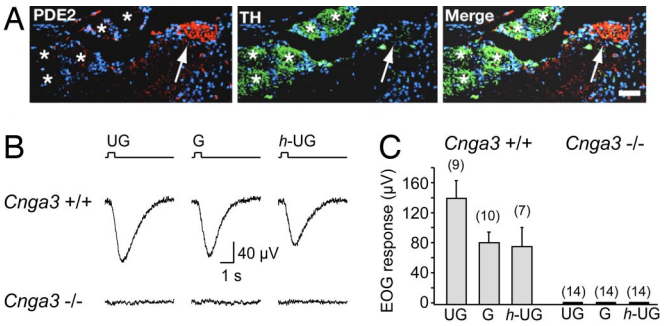

Fig. 3. Essential role of CNGA3 in olfactory recognition of guanylin family peptides. (*A*) PDE2 (red) and TH (green) IHC in a *Cnga3* −/− OB; DAPI (blue) labels cell nuclei. Arrow, necklace glomerulus; asterisk, PDE2-negative glomerulus. (Scale bar: 100 μm.) Two glomeruli are slightly torn from the section. (*B*) Local field potentials generated in the MOE of *Cnga3* +/+ and −/− mice in response to 500-ms pulses of 1 μM UG, G, or *h*-UG. (*C*) EOG peak responses in *Cnga3* +/+ (four mice) and −/− (three mice). Numbers of independent recordings are indicated above each bar. Each stimulus was tested in at least three mice. Data are expressed as means ± SEM.

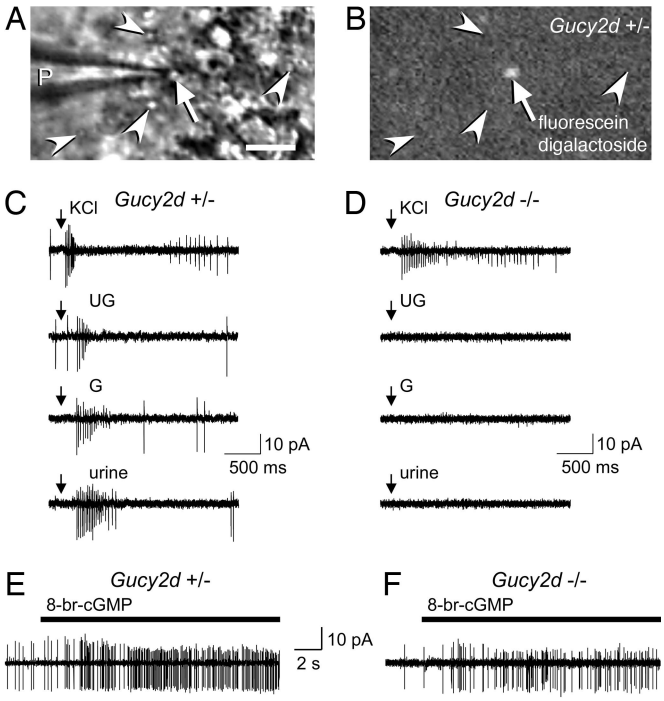

Fig. 4. Patch clamp recording from individual dendritic knobs of GC-D cells. (*A* and *B*) Live cell imaging in intact MOE identifies β-gal-overexpressing OSN knobs. Infrared differential interference contrast (*A*) and fluorescence images (*B*) of the MOE surface (*Gucy2d* +/−) are shown. Several β-gal-negative knobs (arrowheads) surround a single β-gal-positive knob (arrow). P, patch electrode. (Scale bar: 5 μm.) (*C* and *D*) Stimulus-evoked [KCl (60 mM), UG (1 μM), G (1 μM), or dilute urine (1:100)] discharges recorded from β-gal-positive knobs of *Gucy2d* +/− (*C*) or −/− (*D*) mice. Arrows, stimulus application. (*E* and *F*) 8-bromo-cGMP (100 μM) evokes a sustained excitation in β-gal-positive knobs of both *Gucy2d* +/− and −/− mice. Mean spike frequencies after 8-br-cGMP application: 15.4 ± 2.3 Hz (*Gucy2d* +/−, $n = 3$) and 7.8 ± 2.8 Hz (*Gucy2d* −/−, $n = 3$).

reasoned that any candidate ligand would continue to activate the MOE even when the cAMP cascade has been disrupted. By recording local field potentials [the electroolfactogram (EOG)] (12, 25) in *Cnga2*-null mice (26), we found that uroguanylin, a peptide hormone present in urine and associated with the regulation of sodium balance in the gut and kidney through the receptor guanylyl cyclase GC-C (27), elicits a robust electrical response (Fig. 2*B*). The related peptide guanylin (27) produced a similar response (Fig. 2*B*). However, another member of this family, the heat-stable bacterial enterotoxin STp (27), failed to activate the MOE (Fig. 2*B*). The renal natriuretic peptide urodilatin (28), a GC-A agonist, also failed to produce an EOG response (Fig. 2*B*). Uroguanylin- and guanylin-evoked potentials were unaffected by the addition of the adenylyl cyclase inhibitor SQ22536 (300 μM, Fig. 2*C*), confirming their independence from a cAMP signaling mechanism. However, the responses were inhibited by the addition of the CNG channel blocker L-*cis*-diltiazem (29) (100 μM, Fig. 2*C*), implicating another CNG channel, perhaps CNGA3 (17) (see below), in the transduction of uroguanylin and guanylin.

To demonstrate that uroguanylin- and guanylin-evoked potentials are dependent on GC-D, we obtained dose–response measurements in *Gucy2d* +/+, +/−, and −/− mice (Fig. 2 *D–F*). The two peptides were highly potent in the +/+ and +/− mice, with EC_{50} values between 66 and 770 pM (Fig. 2 *D* and *E*). Human uroguanylin, which differs in a number of amino acids from the mouse peptide (Fig. 2*A*), was far less potent than mouse uroguanylin, with a 7- to 36-fold shift of the EC_{50} to higher concentrations (Fig. 2*F*). Thus, variations in ligand structure changed ligand activity. Importantly, responses to each of these ligands were abolished in the *Gucy2d* −/− mice (Fig. 2 *D–F*). Therefore, GC-D is required for the transduction of uroguanylin and guanylin by the MOE.

MOE Responses to Uroguanylin Family Peptides Require CNGA3. In the MOE, the cGMP-specific CNG channel subunit CNGA3 is expressed specifically in GC-D neurons (17). To examine the role of CNGA3 in GC-D neuron function, we used *Cnga3* −/− mice (30), which express GC-D and PDE2 but not CNGA3 in the MOE (SI Fig. 6*C*). Consistent with our observations in *Gucy2d* −/− mice, TH immunoreactivity is nearly absent in PDE2-positive glomeruli in *Cnga3* −/− mice (Fig. 3*A*). Thus, it appears that CNGA3, like GC-D (Fig. 1*C*), is necessary for normal afferent activity to the necklace glomeruli. We next tested the effects of *Cnga3* deletion on uroguanylin and guanylin responses in the MOE. Again consistent with our observations in *Gucy2d* −/− mice, EOG responses to these peptides were abolished in the MOE of *Cnga3* −/− mice (Fig. 3 *B* and *C*). Together, these data indicate that CNGA3 is required for the transduction of uroguanylin and guanylin stimulation of the MOE.

GC-D Neurons Transduce Chemosensory Stimuli with an Excitatory, cGMP-Mediated Mechanism. Mammalian phototransduction involves a receptor guanylyl cyclase, a CNG channel, and the second messenger cGMP. Stimulation of photoreceptors by light results in the hydrolysis of cGMP, the closing of CNG channels, and hyperpolarization of the cell (31). We asked whether uroguanylin and guanylin stimulate or inhibit the activity of individual GC-D neurons. Intact MOE was prepared from the nasal septum of *Gucy2d* +/− or −/− mice, mounted in an *en face* view (32), and imaged by using a combination of infrared differential interference contrast and fluorescence videomicroscopy. The dendritic knobs of β-gal-positive neurons were visualized with the fluorogenic β-gal substrate fluorescein digalactoside and were clearly distinguished from those surrounding knobs that did not express the transgene (Fig. 4 *A* and *B*). Action potentials were measured by obtaining loose patch clamp recordings (33, 34) of labeled knobs. GC-D neurons in *Gucy2d* +/− mice were spontaneously active, with an average spike frequency at rest of 5.7 ± 2.2 Hz ($n = 14$). Spontaneous firing was significantly reduced or eliminated (1.2 ± 1.1 Hz; $n = 6$; $P < 0.001$) in the absence of GC-D, suggesting that basal enzymatic activity of GC-D contributes to setting the resting potential of

NEUROSCIENCE

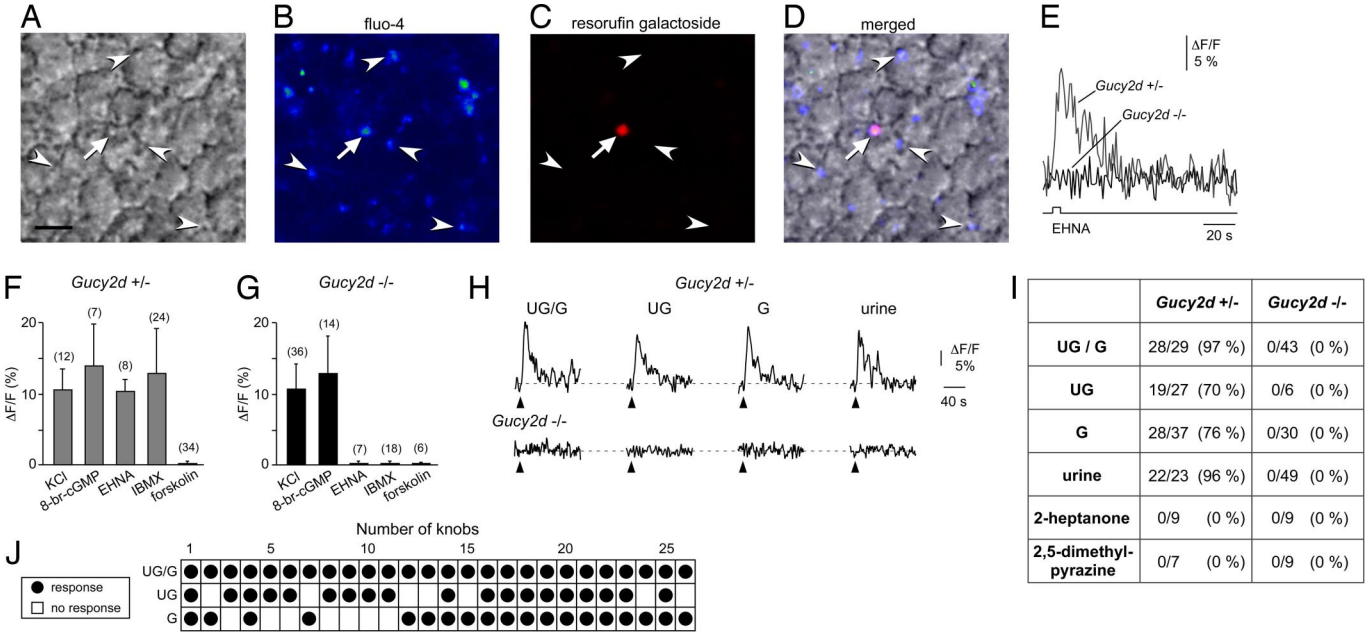

	Gucy2d +/-	Gucy2d -/-
UG / G	28/29 (97 %)	0/43 (0 %)
UG	19/27 (70 %)	0/6 (0 %)
G	28/37 (76 %)	0/30 (0 %)
urine	22/23 (96 %)	0/49 (0 %)
2-heptanone	0/9 (0 %)	0/9 (0 %)
2,5-dimethyl-pyrazine	0/7 (0 %)	0/9 (0 %)

Fig. 5. Confocal imaging of GC-D cell function in intact MOE. (*A–D*) Simultaneous imaging of β-gal and intracellular Ca^{2+} with single-knob resolution: (*A*) transmitted light, (*B*) Ca^{2+} fluorescence acquired at rest, (*C*) β-gal with resorufin galactoside, (*D*) merged. Ca^{2+} fluorescence in a single β-gal-positive knob (arrow; red in *C*, magenta in *D*) within a field of 27 β-gal-negative knobs (some labeled by arrowheads) is shown. (Scale bar: 5 μm.) (*E*) Brief stimulation with PDE2 inhibitor EHNA (50 μM) evokes a Ca^{2+} transient in β-gal-positive knobs of *Gucy2d* +/− but not −/− mice. (*F* and *G*) Histogram summarizing Δ*F*/*F* peak Ca^{2+} responses in *Gucy2d* +/− (*F*) or −/− mice (*G*) to stimulation with 60 mM KCl, 100 μM 8-bromo-cGMP, 50 μM EHNA, 100 μM IBMX, or 20 μM forskolin. The number of experiments is indicated above each bar. (*H*) Example of Ca^{2+} knob responses to UG (1 μM), G (1 μM), UG/G mixture (1 μM each), and urine (1:100). No responses were observed in GC-D cells from *Gucy2d* −/− mice. (*I*) Percentage of β-gal-positive knobs from each genotype that responded to a given stimulus. (*J*) Summary of the response profiles of 26 β-gal-positive knobs (7 *Gucy2d* +/− mice) stimulated successively with a mixture of UG/G as well as single peptides (all at 1 μM). Stimuli were delivered in random order.

these cells. These results also support a role for GC-D in the maintenance of normal afferent activity in the necklace glomeruli (Fig. 1*C*).

GC-D neurons from *Gucy2d* +/− mice were clearly excitable because they responded to extracellular application of 60 mM KCl with a transient rise in spike frequency (Fig. 4*C*). Repeated stimulations with uroguanylin or guanylin (each at 1 μM) produced robust and reproducible increases in spike frequency in these cells (Fig. 4*C*), as did stimulation with the membrane-permeant cGMP analog 8-bromo-cGMP (100 μM, Fig. 4*E*). The probability of evoking peptide-induced responses from randomly selected GC-D cells was unexpectedly high. Of 14 cells stimulated with each peptide sequentially, each showed a guanylin- or uroguanylin-evoked excitation; a large percentage of these cells (6/14, 43%) responded to both peptides (Fig. 4*C*). To support the physiological relevance of these findings, we confirmed that wild-type adult mouse urine (diluted 1:100) also increased spiking of these cells (Fig. 4*C*, $n = 6$). In contrast, only KCl and 8-bromo-cGMP elicited an increase in spike frequency in β-gal-positive neurons from *Gucy2d* −/− mice (Fig. 4 *D* and *F*; $n = 6$), consistent with the field potential recordings (Fig. 2*D*). Thus, GC-D neurons are chemosensory neurons activated by the novel stimuli uroguanylin and guanylin and by a biologically important odor source, urine. Furthermore, these sensory cells, in contrast to mammalian photoreceptors, use an excitatory, cGMP-mediated sensory transduction mechanism.

Optical Imaging of GC-D Cell Function Reveals Unique Receptive Properties. The results described thus far indicate that stimulus encoding by GC-D cells differs sharply from that of canonical OSNs and vomeronasal sensory neurons, where a given molecular cue stimulates only a small fraction of the entire population (4, 12, 33, 34) because of the expression of large numbers of receptors with different receptive properties (2). To provide a quantitative analysis of the diversity of responses across the GC-D neuron population, we next used confocal microscopy of the epithelial sheet (33, 34) to image changes in intracellular Ca^{2+} levels in single dendritic knobs of β-gal-positive neurons. The neuroepithelium was loaded with the Ca^{2+} indicator fluo-4/AM (33, 34), and β-gal-positive knobs were visualized with the fluorogenic substrate resorufin galactoside (Fig. 5 *A–D*). Consistent with our patch clamp results (Fig. 4) and the role of CNGA3 in GC-D-mediated sensory transduction (Figs. 2*C* and 3), dendritic knobs of β-gal-positive neurons in *Gucy2d* +/− mice displayed a rise in intracellular Ca^{2+} upon stimulation with KCl, 8-bromo-cGMP or two highly membrane-permeant PDE inhibitors, the PDE2-selective erythro-9-[2-hydroxy-3-nonyl]-adenine (EHNA) and 3-isobutyl-1-methylxanthine (IBMX) (Fig. 5 *E* and *F*). However, in contrast to its effects on canonical OSNs (12), the adenylyl cyclase activator forskolin did not produce a Ca^{2+} transient in GC-D neurons (Fig. 5 *F* and *G*). This observation is consistent with the absence of adenylyl cyclase and cAMP-sensitive CNG channels in GC-D cells. EHNA- and IBMX-induced Ca^{2+} transients were absent in β-gal-positive neurons of *Gucy2d* −/− mice, although these neurons were still stimulated by KCl and 8-bromo-cGMP (Fig. 5 *E* and *G*). Therefore, we conclude that GC-D is responsible for the cGMP signal in these cells and that the transduction cascade downstream of GC-D remains intact in *Gucy2d* −/− mice.

We next examined Ca^{2+} responses of β-gal-positive dendritic knobs to chemosensory stimuli in *Gucy2d* +/− and −/− mice (58 and 74 knobs, respectively; Fig. 5 *H–J*). In *Gucy2d* +/− mice, nearly 100% of the GC-D neurons tested produced a transient Ca^{2+} elevation to a mixture of uroguanylin and guanylin (Fig. 5 *H–J*). Dilute urine evoked a response with the same high probability (Fig. 5*I*). Even when we applied only a single peptide,

the probability of evoking a response was still remarkably high (70–76%; Fig. 5*I*). However, in no case did we observe a Ca^{2+} response to urine or peptide ligands in *Gucy2d* −/− mice (Fig. 5*I*), although β-gal-positive cells were KCl- and 8-bromo-cGMP-responsive in these mice (Fig. 5*G*). We also never observed a Ca^{2+} response to uroguanylin or guanylin in any β-gal-negative neuron, attesting to the exceptional selectivity of these two peptides for GC-D cells. Although GC-D cells have been suggested to detect some small volatile urinary pheromones such as 2-heptanone and 2,5-dimethylpyrazine (11), we never observed β-gal-positive knobs of *Gucy2d* +/− mice respond to either of these two chemicals with either a Ca^{2+} rise ($n = 16$, Fig. 5*I*) or an increase in action potential frequency ($n = 11$, data not shown).

On a finer scale we did observe some heterogeneity among GC-D cells in *Gucy2d* +/− mice. This observation, first suggested in the knob patch clamp recordings (Fig. 4), was clearly apparent when cells were characterized by Ca^{2+} imaging: whereas the peptide mixture stimulated virtually all GC-D neurons, the individual peptides stimulated subsets of GC-D neurons that only partially overlap (Fig. 5*J*). Therefore, GC-D neurons can be divided into at least three functional classes based on peptide recognition profiles: guanylin-sensitive/uroguanylin-insensitive (7/26, 27%), uroguanylin-sensitive/guanylin-insensitive (7/26, 27%), and guanylin- and uroguanylin-sensitive (12/26, 46%) (Fig. 5*J* and SI Fig. 9). Imaging GC-D cell function at cellular resolution in *Gucy2d* −/− mice revealed that the recognition of single peptide ligands is abolished as a whole (Fig. 5*I*), indicating that GC-D plays an essential role in mediating peptide responsivity in all three functional classes of GC-D neurons.

Discussion

By combining gene-targeting methods with high-resolution electrophysiological and optical imaging techniques in intact MOE, we performed a systematic functional analysis of a unique cellular subpopulation in the mammalian MOE, the GC-D neurons. Our work establishes these cells as extremely sensitive chemodetectors and provides critical insight into the function of a cAMP-independent signal transduction mechanism in the MOE. The ability to image, with single-dendritic knob resolution and in real time, stimulus-induced activity in sparsely distributed, identified neuronal populations of the MOE opens up new areas of investigation in the peripheral olfactory system of mammals.

Our analyses of *Gucy2d* +/− and −/− mice, together with measurements performed in *Cnga2* and *Cnga3* null mice, provide several lines of evidence that the GC-D cells employ a cGMP-dependent second messenger cascade for chemosensory transduction. Furthermore, our data show that not only is this cascade responsible for action potential generation and intracellular Ca^{2+} elevation in these cells but that modulation of GC-D by peptide ligands alters these signals. For example, uroguanylin and guanylin responses are unaffected by the perturbation of the canonical OSN cAMP signaling cascade either by inhibition (Fig. 2*C*) or activation (Fig. 5*F*) of adenylyl cyclase or by deletion of CNGA2, the functionally critical subunit of the olfactory cAMP-gated channel (35) (Fig. 2*B*). Uroguanylin- and guanylin-dependent responses are absent in *Gucy2d* −/− and *Cnga3* −/− mice (Figs. 2*D*, 3*B*, 3*C*, 4*D*, and 5*I*), whereas in *Gucy2d* +/− mice they are reduced by the CNG channel blocker, L-*cis*-diltiazem (Fig. 2*C*) and mimicked by the PDE inhibitors IBMX and EHNA (Fig. 5 *E* and *F*). 8-bromo-cGMP stimulates GC-D neurons in both *Gucy2d* +/− and −/− mice (Figs. 4 *E* and *F* and 5 *F* and *G*) because this cGMP analog bypasses the guanylyl cyclase GC-D in the signaling cascade to gate the CNG channel in these cells directly. Thus, a second cyclic nucleotide-based signaling system, which depends on elevation of cGMP, not cAMP, is used for chemodetection by the MOE.

The excitatory cGMP cascade mediating sensory responses in GC-D neurons differs critically from that of vertebrate retinal photoreceptors because stimulation of those sensory cells by light leads to the G protein activation of a PDE, hydrolysis of cGMP, closing of CNG channels, and a graded membrane hyperpolarization (31). In contrast, stimulation of GC-D neurons leads to membrane depolarization and an increase in action potential frequency (Fig. 4). Interestingly, photoreceptors of the lizard parietal eye also show cGMP-dependent depolarizing responses to sensory stimulation, although this pathway depends on the G protein-dependent inhibition of PDE activity (36). The modulation of GC-D neuronal firing, rather than graded changes in membrane voltage, represents the critical signal processed in the necklace glomeruli of the OB. We cannot distinguish between a model in which direct modulation of GC-D is responsible for information flow and an alternative scenario in which a separate G protein-coupled receptor and downstream effectors impinge on the GC-D pathway. Regardless, our studies demonstrate that the GC-D protein is an essential component for signaling in these cells and that peptide ligands modulate physiological responses to produce signals detected in the target tissue.

A surprising finding was that the GC-D cells are highly sensitive detectors of two peptide hormones, uroguanylin and guanylin, both of which are known to elevate cGMP levels in several tissues (27). Both peptides are secreted from intestine and influence salt and water transport in intestine and kidney (37). GC-D cells are also excited by dilute urine from mature males and females. Uroguanylin is present in relatively high concentrations in urine (27) and may also be present in feces. Guanylin is degraded by chymotrypsin in different parts of the kidney (37), but its presence in urine, at least at low concentrations, cannot be ruled out. Notably, a third member of this peptide family, the heat-stable *Escherichia coli* enterotoxin STp, was ineffective as a chemostimulus for GC-D cells. This latter finding might argue against a possible function of GC-D cells as detectors of pathogenic bacteria, unlike a previously characterized olfactory pathway in *Caenorhabditis elegans* (38).

The mechanisms used for olfactory coding by the GC-D cells also differ sharply from those used by canonical OSNs or vomeronasal sensory neurons. Most notably, our results indicate that a mixture consisting of only two peptide ligands can activate virtually all GC-D neurons, and stimulation with a single peptide activates almost 75% of the cells (Fig. 5 *I* and *J*). This remarkable uniformity is consistent with a model in which GC-D itself functions as the peptide receptor. Other receptor guanylyl cyclases do function as peptide receptors: GC-A and GC-B exhibit differential sensitivities to natriuretic atriopeptins, including atrial natriuretic peptide and urodilatin, whereas GC-C responds to guanylin, uroguanylin, and the enterotoxin STp (24). However, the differential stimulus tuning of GC-D neurons suggests that at least two receptors or receptor variants are expressed across this subpopulation (one activated by uroguanylin only, the other activated by guanylin only). Because receptor guanylyl cyclases commonly function as dimers (24), GC-D could form a common heterodimeric receptor partner to other receptor guanylyl cyclases or similar proteins that are differentially expressed across the population. This possibility seems doubtful, however, because homomeric receptor guanylyl cyclases would likely also be expressed in GC-D neurons, conferring sensitivity to STp, urodilatin, or other peptides that do not stimulate these cells, or maintaining uroguanylin and guanylin sensitivity in *Gucy2d* −/− mice. Alternative splicing of *Gucy2d* might account for the differential selectivity of GC-D receptors. However, we have found no evidence for this possibility (data not shown).

Previous experiments analyzing odor-induced activity in the OB or the effects of genetic ablations suggested an involvement

of the necklace glomeruli in the detection of suckling pheromones (18, 39–41). However, *Gucy2d* −/− mice exhibited no obvious defects in suckling effectiveness (SI Fig. 7), nor did they show any obvious mating defects. Although we cannot yet determine the exact biological function of this olfactory subsystem, the chemostimuli identified here suggest an association with the detection of information related to metabolic status, specifically to regulatory mechanisms that mediate the integration of salt and water balance. It will be interesting to see whether higher neuronal projections from the necklace glomeruli link the GC-D cells with hypothalamic nuclei involved in the control of extracellular fluid volume, Na^+ balance, and osmolarity. In any case, our work identifies guanylin and uroguanylin as mammalian semiochemicals that are recognized by a unique olfactory detection system.

Materials and Methods

For more detailed descriptions of the procedures used, see *SI Materials and Methods*.

Gene Targeting. Portions of *Gucy2d* (19) were targeted for replacement with an IRES-*Mapt-lacZ* reporter (25) in mouse embryonic stem cells. Neo-positive clones undergoing homologous recombination were injected into blastocysts, and chimeric animals were obtained. The selection cassette was removed by cre-dependent recombination (42). The relevant Institutional Animal Care and Use Committees approved all procedures.

Immuno- and X-Gal Histochemistry. Frozen sections of MOE or OB from adult *Gucy2d* +/− and −/− mice and *Cnga3* −/− mice (30) were prepared as described previously (25) and then incubated with primary antisera. Immunoreactivity was visualized with Cy2- and Cy3-labeled secondary antibodies and confocal microscopy. X-Gal histochemistry was performed as described previously (26).

Local Field Potential Recording. The submerged EOG technique was used (12, 25) to record local field potentials from the endoturbinates of adult *Gucy2d* +/− and −/−, *Cnga2*-null (26), *Cnga3* −/−, and wild-type mice. Most stimuli and drugs were focally ejected by using multibarrel stimulation pipettes (33); SQ22536 and L-*cis*-diltiazem were applied by bath flow. The spatial distribution of guanylin- or uroguanylin-evoked potentials fell within a broad central zone of the MOE, consistent with previous GC-D *in situ* hybridizations (16). Epithelial hot spots were often found at the dorsal rim of each endoturbinate.

Live Cell Imaging and Single-Knob Electrophysiology. Intact MOE from the nasal septum of adult mice was mounted *en face* (32). Live dendritic knobs expressing the reporter were visualized by using the fluorogenic β-gal substrate fluorescein digalactoside and imaged with infrared differential interference contrast and fluorescence videomicroscopy. Action potential-driven capacitive currents (32–34) were recorded from identified knobs by using patch pipettes.

Simultaneous Imaging of β-Gal and Ca^{2+}. The epithelial preparation was loaded with the Ca^{2+} indicator fluo-4/AM (33, 34). Changes in intracellular Ca^{2+} concentration were imaged in single knobs by using a confocal laser system (33, 34). Simultaneous visualization of β-gal was achieved by coloading the cells with the fluorogenic substrate resorufin galactoside. No spillover of fluo-4 fluorescence onto the resorufin channel (or vice versa) was observed. Urine was freshly collected from adult C57BL/6 mice. We observed no differences in male or female urine on GC-D cell responses. Data are expressed as means ± SD if not otherwise stated.

This paper is dedicated to the late David L. Garbers. We thank L. Forte, M. Spehr, K. Kelliher, M. Kuhn, S. Hattar, S. Vigues, and L. Newman for helpful discussions and A. Gibson and H.-J. Fulle for assistance in early stages of this project. This work was supported by the National Institute on Deafness and Other Communication Disorders/National Institutes of Health (NIH) Grants R03DC04779 and R01DC00563 (to S.D.M.) R01DC05249 (to F.Z.) R01DC003773 (to T.L.-Z.) and R01DC04553 and R01DC008295 (to R.R.R.), National Institute of General Medical Sciences/NIH Grant T32GM008181 (to R.E.C.), Howard Hughes Medical Institute Grants (to D.L.G. and R.R.R.), and Deutsche Forschungsgemeinschaft Grants Sonderforschungsbereich 530 (to F.Z.) and 391 (to M.B.).

1. Buck L, Axel R (1991) *Cell* 65:175–187.
2. Mombaerts P (2004) *Nat Rev Neurosci* 5:263–278.
3. Zufall F, Munger SD (2001) *Trends Neurosci* 24:191–193.
4. Firestein S (2001) *Nature* 413:211–218.
5. Bakalyar HA, Reed RR (1990) *Science* 250:1403–1406.
6. Pace U, Hanski E, Salomon Y, Lancet D (1985) *Nature* 316:255–258.
7. Jones DT, Reed RR (1989) *Science* 244:790–795.
8. Belluscio L, Gold GH, Nemes A, Axel R (1998) *Neuron* 20:69–81.
9. Wong ST, Trinh K, Hacker B, Chan GC, Lowe G, Gaggar A, Xia Z, Gold GH, Storm DR (2000) *Neuron* 27:487–497.
10. Brennan PA, Zufall F (2006) *Nature* 444:308–315.
11. Lin W, Arellano J, Slotnick B, Restrepo D (2004) *J Neurosci* 24:3703–3710.
12. Spehr M, Kelliher KR, Li XH, Boehm T, Leinders-Zufall T, Zufall F (2006) *J Neurosci* 26:1961–1970.
13. Liberles SD, Buck LB (2006) *Nature* 442:645–650.
14. Ache BW, Young JM (2005) *Neuron* 48:417–430.
15. Gold GH (1999) *Annu Rev Physiol* 61:857–871.
16. Fulle HJ, Vassar R, Foster DC, Yang RB, Axel R, Garbers DL (1995) *Proc Natl Acad Sci USA* 92:3571–3575.
17. Meyer MR, Angele A, Kremmer E, Kaupp UB, Muller F (2000) *Proc Natl Acad Sci USA* 97:10595–10600.
18. Juilfs DM, Fulle HJ, Zhao AZ, Houslay MD, Garbers DL, Beavo JA (1997) *Proc Natl Acad Sci USA* 94:3388–3395.
19. Yang RB, Fulle HJ, Garbers DL (1996) *Genomics* 31:367–372.
20. Shinoda K, Ohtsuki T, Nagano M, Okumura T (1993) *Brain Res* 618:160–166.
21. Shinoda K, Shiotani Y, Osawa Y (1989) *J Comp Neurol* 284:362–373.
22. Baker H, Cummings DM, Munger SD, Margolis JW, Franzen L, Reed RR, Margolis FL (1999) *J Neurosci* 19:9313–9321.
23. Baker H, Kawano T, Margolis FL, Joh TH (1983) *J Neurosci* 3:69–78.
24. Gibson AD, Garbers DL (2000) *Annu Rev Neurosci* 23:417–439.
25. Munger SD, Lane AP, Zhong H, Leinders-Zufall T, Yau KW, Zufall F, Reed RR (2001) *Science* 294:2172–2175.
26. Zhao H, Reed RR (2001) *Cell* 104:651–660.
27. Forte LR, Jr (2004) *Pharmacol Ther* 104:137–162.
28. Forssmann W, Meyer M, Forssmann K (2001) *Cardiovasc Res* 51:450–462.
29. Peng C, Rich ED, Varnum MD (2003) *J Biol Chem* 278:34533–34540.
30. Biel M, Seeliger M, Pfeifer A, Kohler K, Gerstner A, Ludwig A, Jaissle G, Fauser S, Zrenner E, Hofmann F (1999) *Proc Natl Acad Sci USA* 96:7553–7557.
31. Fain GL (2003) *Sensory Transduction* (Sinauer Associates, Sunderland MA).
32. Ma M, Chen WR, Shepherd GM (1999) *J Neurosci Methods* 92:31–40.
33. Leinders-Zufall T, Lane AP, Puche AC, Ma W, Novotny MV, Shipley MT, Zufall F (2000) *Nature* 405:792–796.
34. Leinders-Zufall T, Brennan P, Widmayer P, Chandramani PS, Maul-Pavicic A, Jager M, Li XH, Breer H, Zufall F, Boehm T (2004) *Science* 306:1033–1037.
35. Brunet LJ, Gold GH, Ngai J (1996) *Neuron* 17:681–693.
36. Xiong WH, Solessio EC, Yau KW (1998) *Nat Neurosci* 1:359–365.
37. Sindic A, Schlatter E (2007) *Curr Opin Nephrol Hypertens* 16:10–15.
38. Zhang Y, Lu H, Bargmann CI (2005) *Nature* 438:179–184.
39. Teicher MH, Stewart WB, Kauer JS, Shepherd GM (1980) *Brain Res* 194:530–535.
40. Greer CA, Stewart WB, Teicher MH, Shepherd GM (1982) *J Neurosci* 2:1744–1759.
41. Yagi T, Aizawa S, Tokunaga T, Shigetani Y, Takeda N, Ikawa Y (1993) *Nature* 366:742–745.
42. Schwenk F, Baron U, Rajewsky K (1995) *Nucleic Acids Res* 23:5080–5081.